

Structural Properties of Green Tea Catechins

Dominic Bottin,[†] Giorgia Fugallo,[‡] Franca Fraternali,[§] and Carla Molteni*,[†]

[†]Physics Department, King's College London, Strand, London WC2R 2LS, United Kingdom

[‡]Laboratoire des Solides Irradiés, École Polytechnique, 91128 Palaiseau Cedex, France

[§]Randall Division of Cell and Molecular Biophysics, King's College London, Guy's Campus, London SE1 1UL, United Kingdom

ABSTRACT: Green tea catechins are polyphenols which are believed to provide health benefits; they are marketed as health supplements and are studied for their potential effects on a variety of medical conditions. However, their mechanisms of action and interaction with the environment at the molecular level are still not well-understood. Here, by means of atomistic simulations, we explore the structural properties of four green tea catechins, in the gas phase and water solution: specifically, (−)-epigallocatechin-3-gallate, which is the most abundant, (−)-epicatechin-3-gallate, (−)-epigallocatechin-3-O-(3-O-methyl)-gallate, and (−)-epigallocatechin. We characterize the free energy conformational landscapes of these catechins at ambient conditions, as a function of the torsional degrees of freedom of the polyphenolic rings, determining the stable conformers and their connections. We show that these free energy landscapes are only subtly influenced by the interactions with the solvent and by the structural details of the polyphenolic rings. However, the number and position of the hydroxyl groups (or their substituents) and the presence/absence of the galloyl moiety have significant impact on the selected catechin solvation shells and hydrogen bond capabilities, which are ultimately linked to their ability to interact with and affect the biological environment.



INTRODUCTION

Tea, derived from the plant *Camellia sinensis*, is the second most consumed beverage in the world (behind water) and has been cultivated since ancient times.¹ It has been applied as a cure for many ailments and features prominently in traditional Chinese medicine. In particular, green tea makes up around 20% of worldwide tea production and is prepared in a way which prevents the oxidation and fermentation of the leaf, so that its polyphenolic content is preserved. In fact the alleged health benefits of tea are usually believed to derive from the high concentration of polyphenol flavanoids, including the group known as catechins. These are characterized by the presence of a benzopyran structure bearing at least one aromatic ring and are known for their antioxidant and anti-inflammatory properties.² A number of studies have suggested that green tea catechins may be beneficial to combat depression,^{3–5} influenza,⁶ HIV,^{7,8} obesity,⁹ and Parkinson's and Alzheimer's diseases, e.g. by inhibiting amyloid- β fibril formation,^{10–12} several forms of cancers,^{13–17} and cardiovascular diseases.^{18–20} In particular, interest has been placed on EGCg as a calcium desensitizer or regulator when interacting with cardiac muscle troponin, a calcium binding protein involved in heart contractions,^{21–23} for which we have carried out a computational study.²⁴ Recently EGCg has been tested as carrier with therapeutic effects in the delivery of anticancer proteins, enhancing their effectiveness.²⁵ Because of its natural antioxidant properties, green tea extract has been successfully used to extend the shelf life of food products with high propensity to lipid oxidation.²⁶

However, the mechanisms through which green tea catechins affect the body are still not fully understood. These molecules can interact with biological matter in different ways, depending on concentration and cell type. They are well-known powerful antioxidants, have metal-chelating properties, and show cell protective effects, but they can also play pro-oxidant and cytotoxic roles in some cellular contexts. They can interact directly with molecular targets such as proteins and phospholipids, regulate signal transduction pathways, and modulate enzymes,^{27,28} and they have a strong affinity with lipid bilayers, which may facilitate their entry into cancer cells.²⁹ Overall, the picture is very complex, further complicated by the fact that most of the proposed molecular mechanisms are based on *in vitro* studies at catechin concentrations far in excess of those achievable *in vivo*.^{30,31} Hence it is important to gain insights into these molecules' properties as a first step to elucidate their interactions with complex biological environments. Understanding precisely the structure–function relationship and the role of chemical groups can be ultimately useful for the rational design of catechin-inspired compounds with specific beneficial properties.^{28,30,31}

The goal of this paper is to characterize selected green tea catechins from the structural point of view in the gas phase and in aqueous solution with computational techniques, including molecular dynamics (MD) and metadynamics, an enhancing sampling method to efficiently explore free energy land-

Received: September 7, 2015

Published: September 14, 2015

scapes.^{32,33} Simulations allow us to interrogate the molecules at the atomic scale, giving quantifiable values for properties of interest such as the relative energetics of conformers, hydrogen bond interactions, and solvation shells. Indeed, it has been shown that solvent effects can have significant impacts on the stability of catechins.³⁴

Though several catechins are present in small quantities, by far the most abundant of the green tea polyphenols by weight is (−)-epigallocatechin-3-gallate or EGCg. It is thought that about 80–100 mg of polyphenols are contained in one bag of green tea of which EGCg accounts for 25–30 mg. EGCg is shown in Figure 1 and includes a benzenediol ring (labeled A) joined to a

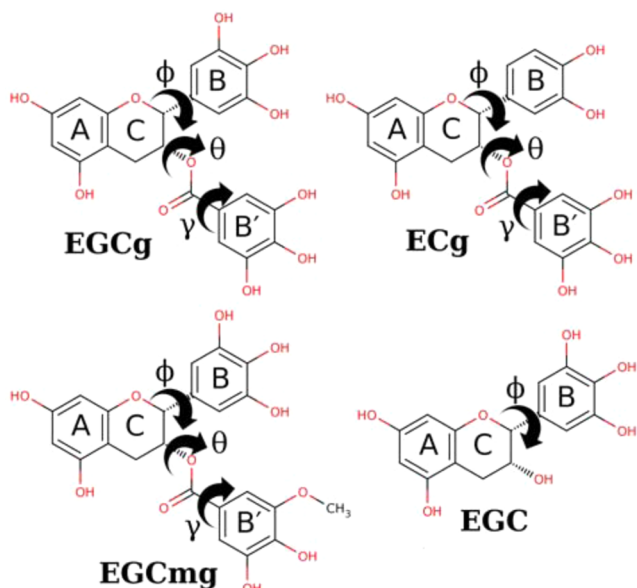


Figure 1. Selected green tea catechins: (−)-epigallocatechin-3-gallate (EGCg), (−)-epicatechin-3-gallate (ECg), (−)-epigallocatechin-3-O-(3-O-methyl)-gallate (EGCmg), and (−)-epigallocatechin (EGC). Rings and torsional angles of interest are labeled.

tetrahydropyran moiety (C), a pyrogallol ring (B), and a galloyl group (with the B' ring).³⁵ The main torsional angles that determine the orientation of the rings and the conformers of the molecule are also labeled as ϕ , θ , and γ . EGCg has been described as the most efficacious of the green tea catechins and is the primary component of green tea extract, commonly found in health shops as a supplement. Hence, the majority of the research attempting to analyze the effects of green tea has concentrated on this molecule. However, for comparison, we selected three other representative, although less abundant, catechins. These are also shown in Figure 1 and are characterized by different side groups that result in different potential interactions with the solvent or biological environment. Specifically, they are (−)-epicatechin-3-gallate (ECg), which lacks a hydroxyl group on the pyrogallol B ring; (−)-epigallocatechin-3-O-(3-O-methyl)-gallate (EGCmg), with a methoxyl rather than a hydroxyl group on the galloyl B' ring; and (−)-epigallocatechin (EGC) where the galloyl group is replaced by a hydrogen atom.

The structural features of green tea catechins that significantly contribute to their biological action are the number and positions of the hydroxyl groups (or their substituents) on the rings, which determine their ability to interact with biological matter through hydrogen bonding, or

electron and hydrogen transfer processes within their antioxidant activities, and by the presence/absence of the galloyl moiety, which clearly distinguishes EGC from the other three catechins. Hence the selected catechins represent a meaningful set to study and compare.

METHODS

As reference, we first calculated the energy profile of the selected catechins as a function of the torsional angles ϕ , θ , and γ in Figure 1, which determine the relative orientation of the polyphenolic rings, at the density functional theory level (DFT), with the B3LYP exchange and correlation functional^{36,37} and the 6-311++G(d,p) basis set,^{38,39} using the GAUSSIAN09 code.⁴⁰ The hybrid B3LYP functional was chosen due to its wide applicability to systems of chemical and biological interest. Each torsional angle was changed and constrained in intervals of 22.5°, while the other two were constrained at specific values ($\phi = 90^\circ$, $\theta = 112.5^\circ$, and $\gamma = 90^\circ$), and the structures were fully relaxed.

Single point Møller–Plesset calculations truncated to second order (MP2) on selected B3LYP structures, corresponding to the γ maxima and minima, were done for comparison, giving consistent results to the DFT data within fractions of kcal/mol. We also tested that the inclusion of dispersion corrections^{41–43} did not change the data significantly, with results very similar to those of MP2. All the catechin profiles showed similar characteristics; however, EGC lacks both the θ and γ angles due to the absence of the galloyl group, so only the energy profile as a function of ϕ could be calculated.

Eight optimized B3LYP structures (two for EGC because of the lack of the θ and γ torsions), corresponding to energy minima at specific torsional angles, were selected to determine partial charges for the parametrization of a classical force field within the General Amber Force Field (GAFF).^{44,45} The partial charges were calculated with a two-step restrained electrostatic potential (RESP) fitting procedure, based upon a set of ESP charges at the Hartree–Fock level of theory for consistency with GAFF. The Hartree–Fock calculations were carried out with the 6-311++G(d,p) basis set, using the GAUSSIAN09 code.⁴⁰ The other force field parameters for the catechins were determined so as to mimic the DFT torsional profiles. Particular attention had to be paid to reproduce the barrier heights of the γ torsion, which, with the default GAFF value, occurred at the correct angular positions but were overestimated by a factor of 4. This was due to the lack of a specific dihedral parameter in GAFF for atom types Os–C–Ca–Ca which was automatically replaced by a default X–C–Ca–X value derived from C₆H₆. Hence a new dihedral parameter was generated to more accurately describe the corresponding torsional potential

$$V_{\text{tors}} = \frac{\text{PK}}{\text{IDIVF}}(1 + \cos(n\phi - \text{phase}))$$

where IDIVF = 1, PK = 1.1 kcal/mol, phase = 180°, and $n = 2$. This gave barrier heights for the γ torsion within 1.5 kcal/mol of the MP2 and B3LYP values. Despite small energy differences in absolute barrier heights, the classical parametrization appeared to reproduce the characteristics of the reference DFT torsional potential energy profiles well and could therefore be confidently used for further dynamical simulations.

Using the AMBER12 package,⁴⁶ we carried out molecular dynamics and metadynamics simulations for the four catechins in the gas phase and water solution. Additional molecular

dynamics simulations were performed in chloroform to contrast the effect of a hydrophilic and hydrophobic environment (different from vacuum). A 10 Å buffer of TIP3P water molecules⁴⁷ or chloroform molecules around the catechins was included in periodically repeated truncated octahedral supercells. The time step for the simulations *in vacuo* was 0.5 fs. For the solvated systems, stretching of the bonds containing hydrogens was restrained with SHAKE,⁴⁸ allowing a 2 fs time step. A Langevin thermostat⁴⁹ with a 1 ps⁻¹ collision frequency was used to maintain the temperature at 300 K, and when the solvent was present, a Berendsen barostat⁵⁰ was also employed to keep the pressure at 1 bar (using a relaxation time of 1 ps).

To fully explore the conformations of the catechins, metadynamics simulations^{32,33} in the gas phase and water were performed. The three torsional angles ϕ , θ , and γ were used as collective variables (CVs), and the dynamics in the space of these CVs was biased by a history dependent potential built as a sum of Gaussians centered in the points of the CV space already visited by the system. This allowed the system to escape from free energy minima and overcome barriers that would have been too high to cross for conventional MD; the free energy landscape could then be reconstructed as a function of the three CVs. The well-tempered metadynamics scheme, which reduces Gaussian height in flat configurational space,⁵¹ was chosen in order to minimize the error in free energy landscape reconstruction, using the PLUMED plugin.⁵² Gaussian width and initial height were set to be 10° and 0.1 kcal/mol, respectively; Gaussians were deposited every 500 time steps. The initial configurations for metadynamics were chosen to be the equilibrated catechin configurations from conventional MD. Earlier analysis of the torsional barriers (with values about 8–12 kcal/mol) suggested the choice of a bias factor of 15. Free energy landscape reconstructions were undertaken after 500 000 and 300 000 Gaussians were deposited for the simulations with three CVs, reduced to 200 000 and 100 000 for EGC, *in vacuo* and water, respectively. Convergence was checked by monitoring the diffusivity of the CVs as well as the evolution of the profiles at regular intervals to make sure that no significant changes occurred in the final part of the simulations. Each reconstructed profile was averaged over 1000 profiles: this combined with the well-tempered metadynamics scheme acted to further reduce the associated error in the free energy to fractions of kcal/mol. To facilitate visualization, the three-dimensional free energy landscapes were projected onto two-dimensional free energy maps (FEM), e.g.

$$\text{FEM}(\gamma, \phi) = -K_B T \ln\left(\int_{-\pi}^{\pi} e^{-F(\gamma, \theta, \phi)/(K_B T)} d\theta\right)$$

or one-dimensional profiles (FEP) such as

$$\text{FEP}(\gamma) = -K_B T \ln\left(\int_{-\pi}^{\pi} \int_{-\pi}^{\pi} e^{-F(\gamma, \theta, \phi)/(K_B T)} d\theta d\phi\right)$$

Molecular dynamics simulations for 50 ns were carried out starting from the minimal energy conformers, *in vacuo*, in water and, for further comparison, in chloroform. As the behavior observed in chloroform during the MD was very similar to that *in vacuo*, with no relevant differences, no metadynamics simulation in chloroform was performed. Statistics were calculated over the last 45 ns of simulations. Properties such as inter- and intramolecular hydrogen bonds and radial distribution functions (RDFs) of catechin oxygens with water oxygens were analyzed, providing a measure of solvent accessibility. The labels for the catechin oxygens used in the

molecular dynamics analysis are shown in Figure 2. The geometrical criteria for defining hydrogen bonds between the

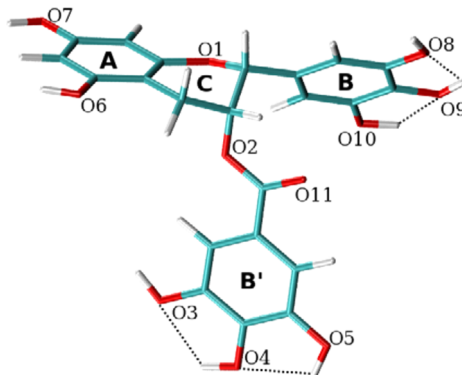


Figure 2. EGCg with labeled oxygens. In ECg the hydroxyl group containing O8 is replaced by a single hydrogen, while in EGCmg O3 has a methyl group bound to it instead of the hydrogen. In EGC the galloyl group attached to O2 is replaced by a hydrogen. Intramolecular hydrogen bonds are indicated with dotted lines.

catechins and water molecules were a donor–acceptor distance smaller than 3.5 Å and a donor–hydrogen–acceptor angle larger than 120°. From examination of the minimized positions of the ring hydroxyl groups as well as their angular fluctuations *in vacuo* and solvent during MD, it appeared that the optimal intramolecular hydrogen bond geometry, as shown in Figure 2, occurred when the donor–hydrogen–acceptor angle was ~110°, and so the intramolecular hydrogen bond analysis was also carried out with an angular cutoff of 100°.

RESULTS AND DISCUSSION

Well-tempered metadynamics simulations were carried out at ambient conditions for each of the catechins, using the ϕ , θ , and γ torsional angles as collective variables in the gas phase and water solution. This allowed the production of free energy surface maps (as a function of two CVs, integrating out the third) and profiles (as a function of one CV, integrating out the other two), which give insights into the conformational free energy landscape of these molecules. Results are shown in Figures 3–5, where the minima and maxima and available pathways to rotation can be seen. It has to be taken into account that they are projections since the free energy landscape as a function of all three CVs is difficult to visualize, but they retain the important information about the free energy minima and features. The locations of the minima and maxima were the same for all the catechins and were not shifted by solvent effects: γ had two equivalent minima at 0° and 180° separated by (projected) barriers of 7–8 kcal/mol; ϕ had two minima at −90° and 90° separated by barriers of less than 4 kcal/mol; θ had two low energy minima around 90° and 160°, separated by a very small barrier of less than 2 kcal/mol, that could easily interconvert at finite temperature, and a less accessible higher energy minimum close to −65°, separated by an anticlockwise barrier of the order of 10 kcal/mol and by a lower clockwise barrier of about 8 kcal/mol. Given the size of the barriers, in molecular dynamics simulations with a reasonable time scale, transitions between the two γ minima and to the higher energy θ minimum could not be observed, while interconversions between the two lower energy θ minima and the two ϕ minima could be easily sampled. Solvent effects, due to the competition between intramolecular and inter-

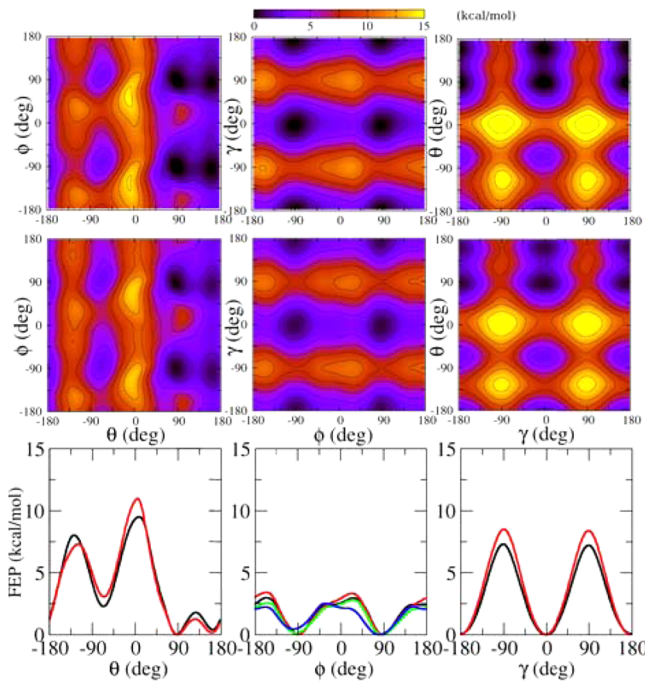


Figure 3. Free energy surface maps at 300 K as a function of the torsional angles θ , ϕ , and γ for EGCg in the gas phase (top panels) and water solution (middle panels) from metadynamics simulations; contour spacing is every 2 kcal/mol. Free energy profiles (FEP, bottom panel) as a function of each torsional angle in the gas phase (red line) and water solution (black line) for EGCg. Free energy profiles as a function of the ϕ torsional angle for EGC (bottom central panel) in the gas phase (blue line) and water solution (green line). The zero of the free energy scale is at the free energy absolute minimum for maps and profiles, respectively.

molecular hydrogen bonds involving the multiple hydroxyl groups present on the B and B' rings, were subtle: they made the two low energy minima in the θ torsion more defined, slightly enhancing the barrier in between them, while in other cases (e.g., in the γ and ϕ profiles and the θ torsional barrier at 0°) they reduced the energy penalty to rotation by as much as 1.5 kcal/mol. In the case of ECg, where the B ring is asymmetric because of the lack of a hydroxyl group, the free energy difference between the two ϕ minima was reduced in water. However, overall the effect of substituents on the B ring in EGc and on the B' ring in ECGmg did not seem to greatly impact the torsional profiles themselves. In fact inter-ring interactions were not changed or enhanced, remaining nonexistent or minimal, with a very slight interaction of the EGCmg methoxyl group on ring B' with ring B, which affected the energy barriers very slightly. The free energy profile of EGC in Figure 3, directly calculated with metadynamics with the single ϕ CV, indicates that the rotation of the B ring is relatively unaffected by the presence or absence of the B' ring for the catechins as the two rings do not interact with each other, except for the slight interaction just mentioned in the case of EGCmg. For EGC the presence of solvent shifts the ϕ maxima from -30° *in vacuo* to +30°. This switching effect is not seen with the projected free energy profiles of the other catechins and is in any case a small difference of about 0.5 kcal/mol. As for the other catechins, these results highlight the fine-tuning of the free energy profiles determined by the available intermolecular interactions with the solvent.

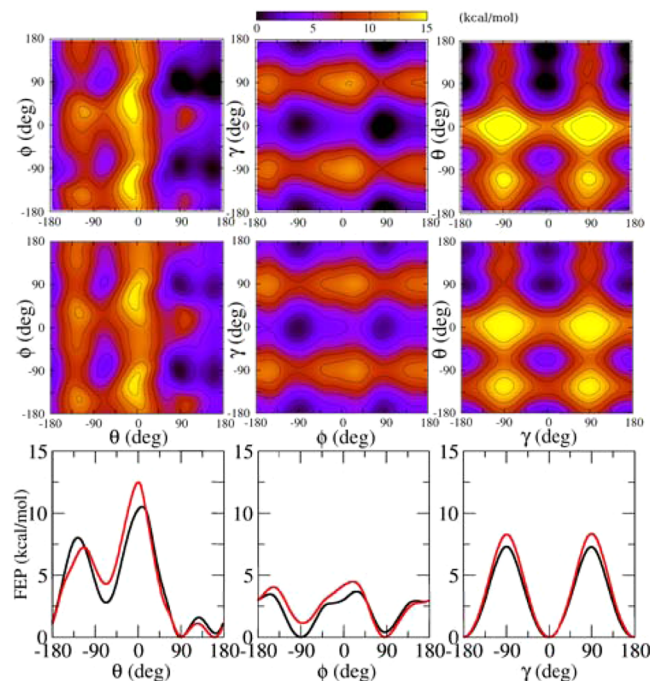


Figure 4. Free energy surface maps at 300 K as a function of the torsional angles θ , ϕ , and γ for ECg in the gas phase (top panels) and water solution (middle panels) from metadynamics simulations; contour spacing is every 2 kcal/mol. Free energy profiles (FEP, bottom panels) as a function of each torsional angle in the gas phase (red line) and water solution (black line). The zero of the free energy scale is at the free energy absolute minimum for maps and profiles, respectively.

We then performed molecular dynamics simulations starting from the lowest free energy minimal structures for the four catechins in the gas phase and in solution; we tested both water and chloroform for a comparison between a hydrophilic and a hydrophobic solvent, as well as vacuum. Consistently with the free energy landscape obtained with metadynamics, γ fluctuated about 0°, θ interconverted between the two minima at 90° and 160°, and ϕ interconverted between the two minima at ±90°.

The average numbers of hydrogen bonds are reported in Table 1, while in Figure 6 the average numbers of hydrogen bonds per catechin oxygen are shown. All intramolecular hydrogen bonds are attributed to the acceptor oxygen to prevent double-counting. Through hydrogen bond analysis, it was observed that intramolecular hydrogen bonding readily occurs on the 3,4,5-trihydroxyl groups for EGCg which can form a maximum of four (two adjacent in the B ring and two adjacent in the B' ring), as shown in Figure 2. For ECg, EGCmg, and EGC structural differences lead to some variations in the intramolecular hydrogen bond numbers as we would expect; they can in fact form a maximum of three (one on the B ring and two in the B' ring), four (two in the B ring and two in the B' ring, although O3 can only act as hydrogen bond acceptor), and three (two in the B ring and one between the O2H hydroxyl group attached to ring C and O1), respectively. Self-interactions through hydrogen bonding between rings of the catechins were not observed, indicating that motion of these rings remained relatively independent. EGCg formed on average about 17 hydrogen bonds with water molecules; ECg and EGCmg formed slightly less (16.5), and EGC, without the galloyl group, about 13.

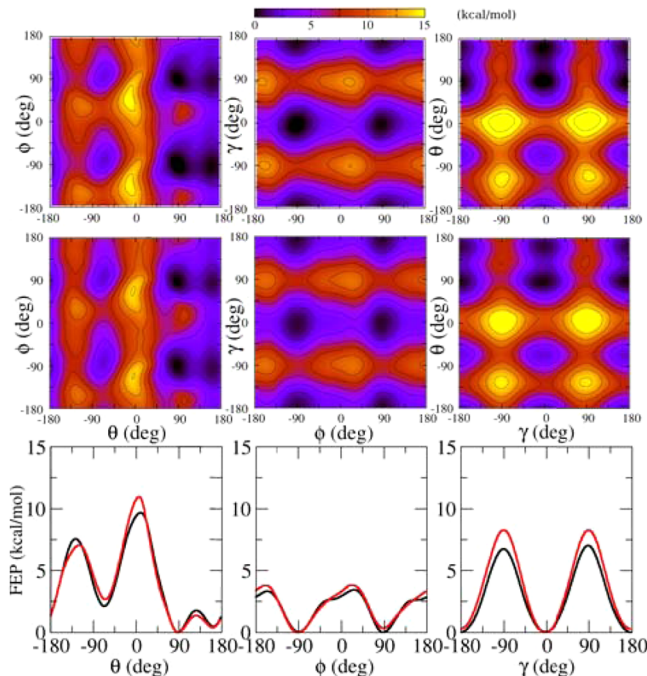


Figure 5. Free energy surface maps at 300 K as a function of the torsional angles θ , ϕ , and γ for EGCmg in the gas phase (top panels) and water solution (middle panels) from metadynamics simulations; contour spacing is every 2 kcal/mol. Free energy profiles (FEP, bottom panels) as a function of each torsional angle in the gas phase (red line) and water solution (black line). The zero of the free energy scale is at the free energy absolute minimum for maps and profiles, respectively.

Table 1. Average Number of Intra- and Intermolecular Hydrogen Bonds During Molecular Dynamics Simulations^a

catechin	intra			inter water
	vacuum	chloroform	water	
EGCg	0.5 (3.8)	0.4 (3.9)	0.3 (3.7)	16.9
ECg	0.7 (2.9)	0.8 (3.0)	0.3 (2.8)	16.5
EGCmg	0.9 (3.9)	0.9 (3.9)	0.5 (3.6)	16.5
EGC	0.3 (2.5)	0.3 (2.5)	0.2 (2.1)	12.9

^aValues in brackets were obtained with a cutoff of 100° rather than 120° for the donor–hydrogen–acceptor angle.

Table 1 depicts several notable trends. The number of the observed intramolecular hydrogen bonds was very similar for the gas phase and the hydrophobic chloroform solvent, with all the possible intraring hydrogen bonds occurring, while the O2H group attached to the tetrahydropyran C ring in ECG formed hydrogen bond with the benzopyran oxygen O1 in ring C about half of the simulation time. In aqueous solution, in spite of the competition with the interaction with water molecules, the average number of intraring hydrogen bonds appeared to decrease only slightly. The occurrence of the hydrogen bond between O2H and O1 in EGC is further reduced; here, O2 formed on average about 2.5 hydrogen bonds with water molecules at variance from the other catechins for which this number was insignificant. The benzopyran oxygen O1, and the two oxygens in the benzenediol A ring (O6 and O7) and O11 (apart from in EGC where it is not present), showed similar hydrogen bond interactions with water in all the analyzed catechins. The two adjacent intraring hydrogen bonds shown in Figure 2 for the

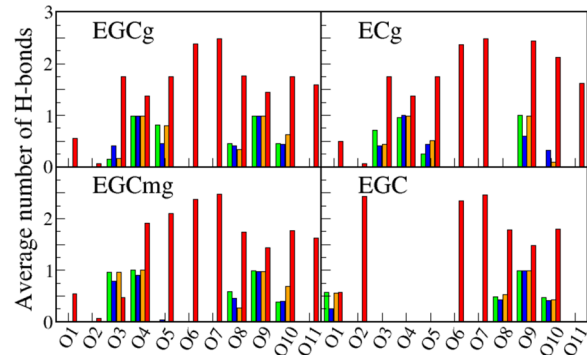


Figure 6. Average numbers of hydrogen bonds formed in MD simulations by each catechin oxygen: green, intramolecular hydrogen bonds *in vacuo*; blue, intramolecular hydrogen bonds in water; yellow, intramolecular hydrogen bonds in chloroform; red, intermolecular hydrogen bonds in water. ECg lacks O8, while EGC lacks O3, O4, O5, and O11. Intramolecular hydrogen bonds were calculated with an angular cutoff of 100°, while intermolecular hydrogen bonds were calculated with an angular cutoff of 120°.

pyrogallol B ring and the galloyl B' ring were the preferred pattern. Figure 6 suggests that they could flip in concert, reversing the donor–acceptor pattern, when all three hydroxyl groups were present in the rings. In EGCg and EGC O4 in the galloyl B' ring always acted as hydrogen bond acceptor (and donor), while O3 and O5 alternated as acceptors (with some preference for one rather than the other pattern possibly due to statistics); intermolecular hydrogen bonds with water were basically identical for this ring. Because O3 in EGCmg is attached to a methyl group and cannot therefore act as donor for hydrogen bonds, the favorable pattern of the intra-B'-ring hydrogen bonds could not flip: in fact O3 and O4 acted as acceptors for about a hydrogen bond each, while O5 behaved like one only with insignificant occurrence. EGCg, EGCmg, and EGC, having an identical pyrogallol B ring, showed very similar behavior concerning both the intra-B-ring and intermolecular hydrogen bonds of this ring with water molecules. In this case, the central oxygen O9 always acted as donor (and acceptor), with O8 and O10 acting as acceptor in alternance, thus allowing the hydrogen bond pattern to flip in concert, similar to the behavior of the galloyl B' ring. In the case of ECg, where O8 is missing, the pattern with an intra-B-ring hydrogen bond where O9 is acceptor seemed to be favored *in vacuo* and in chloroform, although it could flip in water. O9 and O10 formed on average more hydrogen bonds with water molecules with respect to the other catechins, because of the reduced competition with intramolecular hydrogen bonds. In the symmetric B (i.e., when three hydroxyl groups are present, so except for ECg) and B' (again when three hydroxyl groups are present, so except for EGCmg) rings, the same hydrogen bond pattern can be found by flipping in concert the hydrogen bonds in each ring or by rotating each ring by 180° in equivalent position about the ϕ and γ torsional angles, respectively.

Radial distribution functions of catechin oxygens with water oxygens were also calculated and are shown in Figure 7. The RDFs provided insights into the comparative solvent accessibility of the catechins, complementary to the average number of hydrogen bonds. The equivalence of the A ring O6 and O7 was evident from the corresponding RDFs. As they are far from the other aromatic rings, they could interact with water molecules freely (each contributing roughly 2.5 hydrogen bonds to the total catechin–water interactions for each

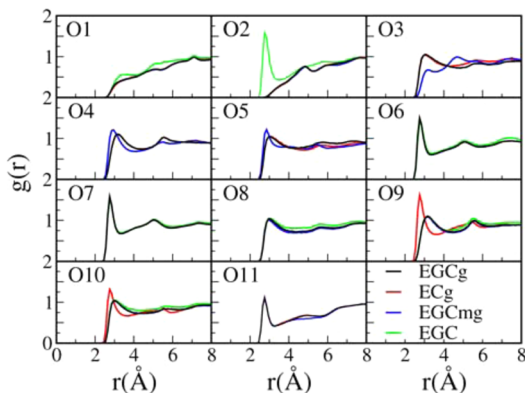


Figure 7. Radial distribution functions between the catechin oxygens and the water oxygens: EGCg (black line), ECg (red line), EGCMg (blue line), and EGC (green line).

catechin) and thus reproduced distinctive first and second solvation shells at 3 and 5 Å, respectively. O11, in the galloyl group which is not present in EGC, also showed very similar behavior for EGCg, ECg, and EGCMg, with a clear peak for the first solvation shell, although lower than in the case of O6 and O7 (in fact accounting for just over 1.5 hydrogen bonds on average); the second solvation shell at 5 Å is just discernible: this could be attributed to the proximity of the A, B, and B' rings which disrupted further water structuring. The three hydroxyl oxygens on the pyrogallol B ring (O8, O9, and O10) and on the galloyl B' ring (O3, O4, and O5) have similar characteristics in that the close proximity of the nearby hydroxyl groups involved in intraring hydrogen bonding reduced the height and sharpness of the first solvation peak with respect to O6/7, while the second peak is less well-defined and at a distance around 5.5 Å. Indeed, for ECg, that lacks O8, the first peak in the RDFs corresponding to O9 and O10, the remaining hydroxyls of the B ring, was sharper due to the diminished competition with intramolecular hydrogen bonds. When the three hydroxyl groups were all present in the pyrogallol B ring and/or galloyl B' ring, the central oxygen (either O9 or O3) showed a more pronounced second solvation shell than the side oxygens. In EGCMg the methyl group attached to O3, which can only act as a hydrogen bond acceptor rather than also as a donor, clearly affected RDFs with respect to O3, but also had an influence on the RDFs with respect to the other two oxygens (O4 and O5) of the galloyl B' ring. In all catechins the O1 oxygen in ring C only interacted minimally with the surrounding waters, which approached it in disordered and unstructured ways. A similar behavior was also seen for O2, except for EGC where the lack of attached galloyl group allowed the (now) hydroxyl group to freely interact with the water solvent: in fact the corresponding RDF resembles that of the O6 and O7 oxygens.

CONCLUSIONS

In this work we characterized four green tea catechins from the structural point of view in the gas phase and in water solution. After parametrizing a suitable force field, we explored their free energy landscape as a function of the ring torsional degrees of freedom. This allowed us to identify minima and maxima and their connections and evaluate the effects of the solvent and of structure modification through ring substituents. We further characterized the minimal free energy structures by carrying out molecular dynamics simulations and analyzing the effects of

solvation through intra- and intermolecular hydrogen bonds and the radial distribution functions; molecular dynamics simulation in chloroform, chosen as a prototypical hydrophobic solvent, gave very similar results to those obtained *in vacuo*.

The water solvent subtly affected the barrier heights in the conformational free energy landscapes as a function of torsional angles, while preserving the location of maxima and minima with respect to the gas phase. Such free energy landscapes were hardly affected by the removal of a hydroxyl group on the pyrogallol B ring in ECg or by substitution of a hydroxyl with a methoxyl group in the galloyl B' ring in EGCMg. Complete removal of the galloyl group in EGC reduced the torsional degrees of freedom only to ϕ , which maintained a free energy profile similar to those of the other catechins, confirming that the polyphenolic B and B' rings can move and act independently.

The similar behavior of the torsional free energy landscapes of the catechins *in vacuo* and water can be attributed to the fact that the torsional angles that characterize the various conformers are in regions of the molecules that are hardly accessed by the solvent and are not influenced by ring details (like side groups). In fact, except for some hydrogen bond interactions with O11, which can explain the observed differences, water molecules approach O1 and O2 in a disordered way and from a distance, without creating persistent hydrogen bonds that would have to be broken and remade during torsions, significantly affecting the free energy landscape. This behavior is evident from the radial distribution functions in Figure 7. For each catechin, the intraring hydrogen bond patterns were seen to persist also in water, although with some small reduction, without preventing the additional intermolecular hydrogen bonds with water molecules.

The torsional barriers of ϕ , which determine the orientation of the B ring, are low, and torsions occur easily, so this ring can orient itself to interact with other molecular systems, either through hydrogen bonding or through electron or hydrogen transfer within antioxidant processes. Similarly, θ can easily swap between its two low energy minima around 90° and 160°, facilitating the repositioning of the galloyl moiety.

The role of the B and B' rings for radical scavenging depends on the specific physiologically relevant radical species (such as superoxide anions, hydroxyl radicals, peroxy radicals, 2,2-diphenyl-1-picrylhydrazyl (DPPH) radicals, singlet oxygens, etc.).²⁶ For example, the hydroxyl groups of the B ring and the galloyl moiety appear to be important for scavenging, respectively, superoxide anions and hydroxyl radicals; both the B and B' rings may be involved in scavenging DPPH radicals, acting somehow independently,⁵³ which is consistent with these rings' independent behavior observed in our simulations. With both the trihydroxyl B ring and the galloyl B' moiety, EGCg was found to be the most effective scavenger for a number of different radical species, including superoxide anions, DPPH, and hydroxyl radicals.⁵³ In other studies the radical scavenging effectiveness was rated largest for ECg followed by EGCg and EGC.³⁰ The pyrogallol group provides EGCg with strong metal-chelating ability, which allows it to bind transition metal ions acting as a preventive antioxidant.^{54,55} The galloyl group has also been associated with inhibitory effects on the microsomal enzyme system^{56,57} as well as with lipid lowering action.²⁷ Hence the galloyl moiety plays a role in enhancing biological activities. While the present study does not address antioxidant properties that need an explicit treatment of the electronic structure, it provides information

about how the rings carrying the hydroxyls can reorient themselves to best interact with the biological environment.

While influencing the torsional free energy landscapes only marginally, the removal and substitutions of side groups in ECg and EGCmg and of the galloyl group in EGC with respect to EGCg significantly affected both the intramolecular and the intermolecular hydrogen bond interactions and the water solvation shells, hence the catechins' ability to interact with the biological environment. In fact, it was found that hydroxyls on the galloyl B' ring showed considerable antiproliferative effects in PC-9 human lung cancer cells,⁵⁸ suggesting that the additional methyl group in EGCmg may disrupt this activity. For ECg the decreased number of hydrogen bonds due to the reduced number of hydroxyl groups on ring B may also be significant as this was seen to decrease the potency of green tea polyphenols in inhibiting lung cancer growth.²⁹ In this respect, EGCmg and ECg could be considered very similar in that they both effectively have one less hydroxyl group which can interact with the environment, which may justify the reduced activity with respect to EGCg in spite of a similar torsional free energy landscape.

In our simulations EGCg formed the largest number of hydrogen bonds in water with respect to the other selected catechins, showing ease of interaction with its surroundings. In biologically relevant situations, the environment can be partially hydrophobic and partially hydrophilic. However, even when binding to the hydrophobic cleft of the C-terminal domain of cardiac muscle troponin C, as studied in our previous work,²⁴ EGCg formed a similar number of hydrogen bonds (16–17, of which 4–5 with the protein and the rest with water). The influence of the number and position of hydroxyl groups and the presence of the galloyl moiety in relation to their hydrogen bonds capabilities was also investigated by molecular dynamics simulations for EGCg interacting with lipid (1-palmitoyl-2-oleoylphosphatidylcholine, POPC) bilayers in comparison with EGC, ECg, EGCg, and epicatechin (EG).⁵⁹

Overall, its largest abundance combined with the presence of both the pyrogallol ring and the galloyl group and the ease and flexibility of interactions with biological matter and solvents are all factors that contribute to the enhanced bioactivity of EGCg with respect to other catechins.

AUTHOR INFORMATION

Corresponding Author

*E-mail: carla.molteni@kcl.ac.uk.

Notes

The authors declare no competing financial interest.

ACKNOWLEDGMENTS

We are grateful for computational support from the UK high performance computing service ARCHER, for which access was obtained via the UKCP consortium and funded by EPSRC grant EP/K013831/1. We also acknowledge the use of the EPSRC UK National Service for Computational Chemistry Software (NSCCS) at Imperial College London (Project ID: CHEM623).

REFERENCES

- (1) MacFarlane, A.; MacFarlane, I. *The Empire of Tea: The Remarkable History of the Plant That Took Over the World*; Overlook Press: Woodstock, NY, 2004.

(2) Kanwar, J.; Taskeen, M.; Mohammad, I.; Huo, C.; Chan, T.; Dou, Q. Recent Advances on Tea Polyphenols. *Front. Biosci., Elite Ed.* **2012**, *4*, 111–131.

(3) Dias, G. P.; Cavegn, N.; Nix, A.; do Nascimento Bevilaqua, M. C.; Stangl, D.; Zainuddin, M. S. A.; Nardi, A. E.; Gardino, P. F.; Thuret, S. The Role of Dietary Polyphenols on Adult Hippocampal Neurogenesis: Molecular Mechanisms and Behavioural Effects on Depression and Anxiety. *Oxid. Med. Cell. Longevity* **2012**, *2012*, S41971.

(4) Mirza, B.; Ikram, H.; Bilgrami, S.; Haleem, D. J.; Haleem, M. A. Neurochemical and Behavioral Effects of Green Tea (*Camellia Sinensis*): A Model Study. *Pak. J. Pharm. Sci.* **2013**, *26*, 511–516.

(5) Zhu, W.-L.; Shi, H.-S.; Wei, Y.-M.; Wang, S.-J.; Sun, C.-Y.; Ding, Z.-B.; Lu, L. Green Tea Polyphenols Produce Antidepressant-like Effects in Adult Mice. *Pharmacol. Res.* **2012**, *65*, 74–80.

(6) Nakayama, M.; Suzuki, K.; Toda, M.; Okubo, S.; Hara, Y.; Shimamura, T. Inhibition of the Infectivity of Influenza Virus by Tea Polyphenols. *Antiviral Res.* **1993**, *21*, 289–299.

(7) Hamza, A.; Zhan, C. How Can (−)-Epigallocatechin Gallate from Green Tea Prevent HIV-1 Infection? *J. Phys. Chem. B* **2006**, *110*, 2910–2919.

(8) Yamaguchi, A.; Honda, M.; Ikigai, H.; Hara, Y.; Shimamura, T. Inhibitory Effects of (−)-Epigallocatechin Gallate on the Life Cycle of Human Immunodeficiency Virus Type 1 (HIV-1). *Antiviral Res.* **2002**, *53*, 19–34.

(9) Wolfram, S.; Wang, Y.; Thielecke, F. Anti-Obesity Effects of Green Tea: from Bedside to Bench. *Mol. Nutr. Food Res.* **2006**, *50*, 176–187.

(10) Ehrnhoefer, D. E.; Bieschke, J.; Boeddrich, A.; Herbst, M.; Masino, L.; Lurz, R.; Engemann, S.; Pastore, A.; Wanker, E. E. EGCg Redirects Amyloidogenic Polypeptides into Unstructured, off-Pathway Oligomers. *Nat. Struct. Mol. Biol.* **2008**, *15*, 558–566.

(11) Bieschke, J.; Russ, J.; Friedrich, R. P.; Ehrnhoefer, D. E.; Wobst, H.; Neugebauer, K.; Wanker, E. E. EGCg Remodels Mature α -Synuclein and Amyloid- β Fibrils and Reduces Cellular Toxicity. *Proc. Natl. Acad. Sci. U. S. A.* **2010**, *107*, 7710–7715.

(12) Zhang, T.; Zhang, J.; Derreumaux, P.; Mu, Y. Molecular Mechanism of the Inhibition of EGCG on the Alzheimer $A\beta(1-42)$ Dimer. *J. Phys. Chem. B* **2013**, *117*, 3993–4002.

(13) Bushman, J. L. Green Tea and Cancer in Humans: a Review of the Literature. *Nutr. Cancer* **1998**, *31*, 151–159.

(14) Rathore, K.; Choudhary, S.; Odoi, A.; Wang, H.-C. R. Green Tea Catechin Intervention of Reactive Oxygen Species-Mediated ERK Pathway Activation and Chronically Induced Breast Cell Carcinogenesis. *Carcinogenesis* **2012**, *33*, 174–183.

(15) Kostin, S. F.; McDonald, D. E.; McFadden, D. W. Inhibitory Effects of (−)-Epigallocatechin-3-Gallate and Pterostilbene on Pancreatic Cancer Growth in Vitro. *J. Surg. Res.* **2012**, *177*, 255–262.

(16) De Amicis, F.; Perri, A.; Vizza, D.; Russo, A.; Panno, M. L.; Bonofoglio, D.; Giordano, C.; Mauro, L.; Aquila, S.; Tramontano, D.; et al. Epigallocatechin Gallate Inhibits Growth and Epithelial-to-Mesenchymal Transition in Human Thyroid Carcinoma Cell Lines. *J. Cell. Physiol.* **2013**, *228*, 2054–2062.

(17) Singh, B. N.; Shankar, S.; Srivastava, R. K. Green Tea Catechin, Epigallocatechin-3-Gallate (EGCg): Mechanisms, Perspectives and Clinical Applications. *Biochem. Pharmacol.* **2011**, *82*, 1807–1821.

(18) Hertog, M. G. L.; Feskens, E. J. M.; Hollman, P. C. H.; Katan, M. B.; Kromhout, D. Dietary Antioxidant Flavonoids and Risk of Coronary Heart Disease: the Zutphen Elderly Study. *Lancet* **1993**, *342*, 1007–1011.

(19) Riemersma, R.; Rice-Evans, C.; Tyrrell, R.; Clifford, M.; Lean, M. Tea Flavonoids and Cardiovascular Health. *Q. J. Med.* **2001**, *94*, 277–282.

(20) Hodgson, J. M. Tea Flavonoids and Cardiovascular Disease. *Asia Pac. J. Clin. Nutr.* **2008**, *17*, 288–290.

(21) Tadano, N.; Du, C.; Yumoto, F.; Morimoto, S.; Ohta, M.; Xie, M.; Nagata, K.; Zhan, D.; Lu, Q.; Miwa, Y.; et al. Biological Actions of Green Tea Catechins on Cardiac Troponin C. *Br. J. Pharmacol.* **2010**, *161*, 1034–1043.

- (22) Robertson, I.; Li, M.; Sykes, B. Solution Structure of Human Cardiac Troponin C in Complex with the Green Tea Polyphenol, (−)-Epigallocatechin 3-Gallate. *J. Biol. Chem.* **2009**, *284*, 23012–23022.
- (23) Messer, A. E.; Marston, S. B. Investigating the Role of Uncoupling of Troponin I Phosphorylation from Changes in Myofibrillar Ca(2+)-Sensitivity in the Pathogenesis of Cardiomyopathy. *Front. Physiol.* **2014**, *5*, 315.
- (24) Botten, D.; Fugallo, G.; Fraternali, F.; Molteni, C. A Computational Exploration of the Interactions of the Green Tea Polyphenol (−)-Epigallocatechin 3-Gallate with Cardiac Muscle Troponin C. *PLoS One* **2013**, *8*, e70556.
- (25) Chung, J. E.; Tan, S.; Gao, S. J.; Yongvongsoontorn, N.; Kim, S. H.; Lee, J. H.; Choi, H. S.; Yano, H.; Zhuo, L.; Kurisawa, M.; et al. Self-Assembled Micellar Nanocomplexes Comprising Green Tea Catechin Derivatives and Protein Drugs for Cancer Therapy. *Nat. Nanotechnol.* **2014**, *9*, 907–912.
- (26) Senanayake, S. N. Green Tea Extract: Chemistry Antioxidant Properties and Food Applications. A Review. *J. Funct. Foods* **2013**, *5*, 1529–1541.
- (27) Kim, H.-S.; Quon, M. J.; Kim, J.-a. New Insights into the Mechanisms of Polyphenols beyond Antioxidant Properties; Lessons from the Green Tea Polyphenol, Epigallocatechin 3-gallate. *Redox Biol.* **2014**, *2*, 187–195.
- (28) Afzal, M.; Safer, A.; Menon, M. Green Tea Polyphenols and their Potential Role in Health and Disease. *Inflammopharmacology* **2015**, *23*, 151–161.
- (29) Okabe, S.; Suganuma, M.; Hayashi, M.; Sueoka, E.; Komori, A.; Fujiki, H. Mechanisms of Growth Inhibition of Human Lung Cancer Cell Line, PC-9, by Tea Polyphenols. *Jpn. J. Cancer Res.* **1997**, *88*, 639–43.
- (30) Braicu, C.; Ladomery, M. R.; Chedea, V. S.; Irimie, A.; Berindan-Neagoe, I. The Relationship between the Structure and Biological Actions of Green Tea Catechins. *Food Chem.* **2013**, *141*, 3282–3289.
- (31) Zaveri, N. T. Green Tea and its Polyphenolic Catechins: Medicinal Uses in Cancer and Noncancer Applications. *Life Sci.* **2006**, *78*, 2073–2080.
- (32) Laio, A.; Parrinello, M. Escaping Free Energy Minima. *Proc. Natl. Acad. Sci. U. S. A.* **2002**, *99*, 12562–12566.
- (33) Laio, A.; Gervasio, F. L. Metadynamics: a Method to Simulate Rare Events and Reconstruct the Free energy in Biophysics, Chemistry and Material Science. *Rep. Prog. Phys.* **2008**, *71*, 126601.
- (34) Monajjemi, M.; Khosravi, M.; Honarpardvar, B.; Mollaamin, F. Substituent and Solvent Effects on the Structural Bioactivity and Anticancer Characteristic of Catechin as a Bioactive Constituent of Green Tea. *Int. J. Quantum Chem.* **2011**, *111*, 2771–2777.
- (35) Balentine, D.; Wiseman, S.; Bouwens, L. The Chemistry of Tea Flavonoids. *Crit. Rev. Food Sci. Nutr.* **1997**, *37*, 693–704.
- (36) Becke, A. Density-Functional Thermochemistry. III. The Role of Exact Exchange. *J. Chem. Phys.* **1993**, *98*, 5648–5652.
- (37) Stephens, P.; Devlin, F.; Chabalowski, C.; Frisch, M. Ab Initio Calculation of Vibrational Absorption and Circular Dichroism Spectra Using Density Functional Force Fields. *J. Phys. Chem.* **1994**, *98*, 11623–11627.
- (38) McLean, A. D.; Chandler, G. S. Contracted Gaussian-Basis Sets for Molecular Calculations. 1. 2nd Row Atoms, Z = 11–18. *J. Chem. Phys.* **1980**, *72*, 5639–5648.
- (39) Krishnan, R.; Binkley, J. S.; Seeger, R.; Pople, J. A. Self-Consistent Molecular-Orbital Methods. 20. Basis set for correlated wave-functions. *J. Chem. Phys.* **1980**, *72*, 650–654.
- (40) Frisch, M. J.; Trucks, G. W.; Schlegel, H. B.; Scuseria, G. E.; Robb, M. A.; Cheeseman, J. R.; Scalmani, G.; Barone, V.; Mennucci, B.; Petersson, G. A.; et al. *Gaussian 09 Revision A.1*; Gaussian Inc.: Wallingford, CT, 2009.
- (41) Grimme, S. Accurate Description of van der Waals Complexes by Density Functional Theory Including Empirical Corrections. *J. Comput. Chem.* **2004**, *25*, 1463–1473.
- (42) Grimme, S. Semiempirical GGA-type Density Functional Constructed with a Long-Range Dispersion Correction. *J. Comput. Chem.* **2006**, *27*, 1787–1799.
- (43) Grimme, S.; Antony, J.; Ehrlich, S.; Krieg, H. A Consistent and Accurate ab Initio Parametrization of Density Functional Dispersion Correction (DFT-D) for the 94 Elements H-Pu. *J. Chem. Phys.* **2010**, *132*, 154104.
- (44) Lindorff-Larsen, K.; Piana, S.; Palmo, K.; Maragakis, P.; Klepeis, J. L.; Dror, R. O.; Shaw, D. E. Improved Side-Chain Torsion Potentials for the Amber ff99SB Protein Force Field. *Proteins: Struct., Funct., Bioinf.* **2010**, *78*, 1950–1958.
- (45) Wang, J. M.; Wolf, R. M.; Caldwell, J. W.; Kollman, P. A.; Case, D. A. Development and Testing of a General Amber Force Field. *J. Comput. Chem.* **2004**, *25*, 1157–1174.
- (46) Case, D.; Darden, T.; Cheatham, I.; Simmerling, C.; Wang, J.; Duke, R.; Luo, R.; Walker, R.; Zhang, W.; Merz, K.; et al. AMBER 12; University of California: San Francisco, CA, 2012.
- (47) Jorgensen, W. L.; Chandrasekhar, J.; Madura, J. D.; Impey, R. W.; Klein, M. L. Comparison of Simple Potential Functions for Simulating Liquid Water. *J. Chem. Phys.* **1983**, *79*, 926–935.
- (48) Ryckaert, J. P.; Ciccotti, G.; Berendsen, H. Numerical Integration of the Cartesian Equations of Motion of a System with Constraints: Molecular Dynamics of n-Alkanes. *J. Comput. Phys.* **1977**, *23*, 327–341.
- (49) Grest, G. S.; Kremer, K. Molecular-Dynamics Simulation for Polymers in the Presence of a Heat Bath. *Phys. Rev. A: At., Mol., Opt. Phys.* **1986**, *33*, 3628–3631.
- (50) Berendsen, H.; Postma, J.; van Gunsteren, W.; DiNola, A.; Haak, J. Molecular Dynamics with Coupling to an External Bath. *J. Chem. Phys.* **1984**, *81*, 3684–3690.
- (51) Barducci, A.; Bussi, G.; Parrinello, M. Well-Tempered Metadynamics: A Smoothly Converging and Tunable Free-Energy Method. *Phys. Rev. Lett.* **2008**, *100*, 020603.
- (52) Bonomi, M.; Branduardi, D.; Bussi, G.; Camilloni, C.; Provasi, D.; Raiteri, P.; Donadio, D.; Marinelli, F.; Pietrucci, F.; Broglia, R. A.; et al. PLUMED: A Portable Plugin for Free-Energy Calculations with Molecular Dynamics. *Comput. Phys. Commun.* **2009**, *180*, 1961–1972.
- (53) Nanjo, F.; Mori, M.; Goto, K.; Hara, Y. Radical Scavenging Activity of Tea Catechins and Their Related Compounds. *Biosci. Biotechnol., Biochem.* **1999**, *63*, 1621–1623.
- (54) Guo, Q.; Zhao, B.; Li, M.; Shen, S.; Xin, W. Studies on Protective Mechanisms of Four Components of Green Tea Polyphenols against Lipid Peroxidation in Synaptosomes. *Biochim. Biophys. Acta, Lipids Lipid Metab.* **1996**, *1304*, 210–222.
- (55) Zhang, G.; Miura, Y.; Yagasaki, K. Suppression of Adhesion and Invasion of Hepatoma Cells in Culture by Tea Compounds through Antioxidative Activity. *Cancer Lett.* **2000**, *159*, 169–173.
- (56) Chen, L.; Zhang, H.-Y. Cancer Preventive Mechanisms of the Green Tea Polyphenol (−)-Epigallocatechin-3-gallate. *Molecules* **2007**, *12*, 946–957.
- (57) Wang, Z. Y.; Das, M.; Bickers, D. R.; Mukhtar, H. Interaction of Epicatechins Derived from Green Tea with Rat Hepatic Cytochrome P-450. *Drug Metab. Dispos.* **1988**, *16*, 98–103.
- (58) Dodo, K.; Minato, T.; Hashimoto, Y. Structure-Activity Relationship of Bis-Galloyl Derivatives Related to (−)-Epigallocatechin Gallate. *Chem. Pharm. Bull.* **2009**, *57*, 190–194.
- (59) Sirk, T. W.; Brown, E. F.; Friedman, M.; Sum, A. K. Molecular Binding of Catechins to Biomembranes: Relationship to Biological Activity. *J. Agric. Food Chem.* **2009**, *57*, 6720–6728.